元吉正樹，藤江正克，他.	磁力駆動手術マニピュレータの開発	日本機械学会[No. 04-4] ロボティクス・メカトロニクス講演会2004 講演論文集		2P2-H-54	2004
原田香奈子，藤江正克，他.	Open-MRI下における低侵襲胎児手術用マニピュレータの開発	第13回日本コンピュータ外科学会論文集		111-112	2004
Harada K, Fujie MG, et al.	Micro manipulators for intrauterine fetal surgery in an Open MRI	ICRA 2005 IEEEInternational Conference on Robotics And Automation		502-507	2005
Harada K, Fujie MG, et al.	Manipulators for intrauterine fetal surgery in an Open MRI-Report on first prototype-	CARS 2005 Computer Assisted Radiology and Surgery		1281	2005
原田香奈子，藤江正克，他.	Open MRI下胎児手術支援システムの開発（第一報）－微細マニピュレータと鉗子ナビゲーション－	日本機械学会ロボティクス・メカトロニクス講演会2005講演論文集		2A1-N-118	2005
元吉正樹，藤江正克.	磁気駆動方式による手術マニピュレータの開発	第14回日本コンピュータ外科学会大会論文集		133-134	2006
元吉正樹，藤江正克，他.	低侵襲手術用磁気駆動方式マニピュレータの開発	日本機械学会ロボティクス・メカトロニクス講演2006講演論文集		2A1-11 (DVD)	2006
Yabukami S, Ishiyama K, Arai K I, et al.	A design of highly sensitive GMI sensor	Journal of Magnetism and Magnetic Materials	290-291	1318-1321	2005
Hashi S, Ishiyama K, Arai, K. I, et al.	Wireless motion capture system using magnetically coupled LC resonant marker	Journal of Magnetism and Magnetic Materials	290-291	1330-1333	2005
堀越直，石山和志，荒井賢一，他.	振幅変調による高周波キャリア型薄膜磁界センサの設計	日本応用磁気学会誌	29	472-476	2005
小澤哲也，石山和志，荒井賢一，他.	高周波キャリアを用いた位相検出型薄膜磁界センサの開発	日本応用磁気学会誌	29	663-666	2005
小澤哲也，石山和志，荒井賢一，他.	高周波キャリア型薄膜磁界センサの位相差検出による交流磁界測定装置の開発	日本応用磁気学会誌	29	831-837	2005
Hashi S, Ishiyama K, Arai K. I, et al.	Development of Real-Time and Highly Accurate Wireless Motion Cupture System Utilizing Soft Magnetic Core	IEEE Transactions on Magnetics	41(10)	4191-4193	2005
仙道雅彦，石山和志，荒井賢一，他.	端部磁性体を配置した高周波キャリア型磁界センサの感度向上に関する研究	日本応用磁気学会誌	30	225-228	2006
村山芳隆，石山和志，荒井賢一，他.	熱処理温度制御による高周波キャリア型薄膜磁界センサの高感度化	日本応用磁気学会誌	30	237-242	2006
豊田征治，石山和志，荒井賢一，他.	複数LC共振型磁気マーカを用いた多点位置検出システム	日本応用磁気学会誌	30	391-395	2006
Hashi S, Ishiyama K, Okazaki Y, Arai K. I, et al.	Wireless Magnetic Motion Capture System for Multi-Marker Detection	IEEE Trans. Magnetics	42(10)	3279-3281	2006

村山芳隆，石山和志，荒井賢一，他.	10-13T 台の磁界検出分解能を有する高周波伝送線路型薄膜磁界センサ	日本応用磁気学会誌	31	17-22	2007
中居倫夫，石山和志，荒井賢一，他.	不連続インピーダンス変化特性を有した薄膜GMI センサと微分回路を組み合わせた磁界検出方法に関する検討	日本応用磁気学会誌	31	216-220	2007
加藤智紀，石山和志，荒井賢一.	形状磁気異方性による高周波キャリア型磁界センサの異方性制御	日本応用磁気学会誌	31	227-230	2007
清嶋護之，雨宮隆太，他.	当院における気道異物症例	気管支学	27(7)	529-532	2005
鏑木孝之，雨宮隆太.	気管支鏡所見の捉え方	気管支学	27(5)	395-400	2005
清嶋護之，雨宮隆太，他.	Virtual bronchoscopy の臨床応用	呼吸器科	8(6)	533-537	2005
Satani T, Amemiya R, et al.	Amyloid deposition in primary pulmonary marginal zone B-cell lymphoma of mucosa-associated lymphoid tissue	Pathology International	57	746-750	2007
土田敬明，他.	縦隔・肺門部病変に対するCTガイド下気管支鏡生検	気管支学	27(2)	110-113	2005
小林寿光，土田敬明，他.	CTガイド下気管支鏡による末梢肺野病変の診断	気管支学	27(4)	302-306	2005
Kobayashi T, Tsuchida, T, et al.	A flexible endoscopic surgical system: First report on a conceptual design of the system validated by experiments	Jpn J Clin Oncol.	35	667-671	2005
中島崇裕，土田敬明，他.	肺癌術前リンパ節転移診断における、コンベックス走査式超音波気管支鏡ガイド下生検(EBUS-TBNA)の実際	肺癌	47	207-214	2007
中馬広一，荒木信人.	骨転移治療の最近の動向　骨転移に対する手術治療の位置付けと今後の展開	癌の臨床	52(13)	857-866	2006
中馬広一.	骨転移による病的骨折，脊髄圧迫症状に対する手術療法	がん患者と対症療法	18(1)	40-46	2007
中馬広一，中谷文彦.	がん骨転移における骨代謝異常	日本臨床	65(9)	543-549	2007
中馬広一，中谷文彦.	悪性骨軟部腫瘍に対する術前治療- 高い治療成績と機能再建を求めた治療法の確立	医学のあゆみ	221(4)	297-302	2007
Kinoshita T, Fukutomi T.	Magnetic resonance imaging of benign phyllodes tumors of the breast	Breast J	10	232-236	2004

Kinoshita T, Fukutomi T, Iwamoto E, et al.	Intracystic papillary carcinoma of the breast in a male patient diagnosed by core needle biopsy: a case report	The Breast	14	322-324	2005
Komoike Y, Akiyama F, Kinoshita T, et al.	Analysis of ipsilateral breast tumor recurrences after breast conserving treatment based on classification of true recurrence and new primary tumors	Breast Cancer	12	104-111	2005
Takasugi M, Iwamoto E, Kinoshita T, et al.	General aspects and specific issues of informed consent on breast cancer treatments	Breast Cancer	12	39-44	2005
Kanazawa T, Kinoshita T, Fukutomi T, et al.	Diagnosis of complete response to neoadjuvant chemotherapy using diagnostic imaging in primary breast cancer patients	Breast J	11	311-316	2005
Kinoshita T, Fukutomi T, et al.	Sentinel lymph node biopsy examination for breast cancer patients with clinically negative axillary lymph nodes after neoadjuvant chemotherapy	The American Journal of Surgery	191	225-229	2006
Yamaguchi J, KinoshitaT, et al.	A Case of mucinous carcinoma of the breast that demonstrated a good pathological response to neoadjuvant chemotherapy despite a poor clinical response	Breast cancer	13	100-103	2006
木下貴之.	術前化学療法後のセンチネルリンパ節生検	乳癌の臨床	21	135-139	2006
Komoike Y, Akiyama F, Kinoshita T, et al.	Ipsilateral breast tumor recurrence (IBTR) after breast-conserving treatment for early breast cancer	Cancer	106	35-41	2006
赤木智徳, 木下貴之.	Intracystic papillary carcinoma (ICPC)の診断と臨床的特徴－自験例14例からの検討－	乳癌の臨床	22(4)	280-285	2007
Akashi TS, Omatsu M, Kinoshita T, et al.	Favorable outcome in patients with breast cancer in the presence of pathological response after neoadjuvant endocrine therapy	The Breast	16	482-488	2007

Kurebayashi J, Kinoshita T, et al.	The prevalence of intrinsic subtypes and prognosis in breast cancer patients of different races	The Breast	16	72-77	2007
Tsukamoto S, Kinoshita T, et al.	Brain metastases after achieving local pathological complete responses with neoadjuvant chemotherapy	Breast Cancer	14(4)	420-424	2007
Kinoshita T.	Sentinel lymph node biopsy is feasible for breast cancer patients after neoadjuvant chemotherapy	Breast Cancer	14(1)	10-15	2007
Takahashi A, Fujimoto H, Nakagawa M, et al.	Radical Cystectomy for Invasive Bladder Cancer: Results of Multi -institutional Pooled Analysis	Jpn J Clin Oncol	34	14-19	2004
Kitamura H, Fujimoto H, Kakizoe T, et al.	Dynamic Computed Tomography and Color Doppler Ultrasound of Renal Parenchymal Neoplasms: Correlations with Histopathological Findings	Jpn J Clin Oncol	34(2)	78-81	2004
Nakagawa T, Fujimoto H, Hasegawa T, et al.	Malignant mixed epithelial and stromal tumours of the kidney: a report of the first two cases with a fatal clinical outcome	Histopathology	44	302-304	2004
藤元博行.	局所進行前立腺癌に対するホルモン療法と手術療法の併用療法	日本臨床	63(2)	271-278	2005
Uchida T, Fujimoto H, Naitoh S, et al.	TRANSRECTAL HIGH-INTENSITY FOCUSED ULTRASOUND IN THE TREATMENT OF LOCALIZED PROSTATE CANCER: A MULTICENTER STUDY	Acta Urol Jpn	51	651-658	2005
藤元博行.	本邦、前立腺癌症例に対する根治的前立腺全摘の可能性と限界	臨床放射線	50(5)	593-601	2005
赤倉功一郎, 藤元博行, 島崎淳.	局所進行前立腺癌に対する根治的前立腺摘除術＋内分泌療法と放射線外部照射＋内分泌療法とを比較する無作為化比較試験の長期成績	泌尿器外科	19(8)	967-969	2006
藤元博行.	非神経温存前立腺広汎切除術における排尿機能	Urology View	5(2)	51-57	2007
藤元博行.	II. 臨床研究　治療　外科治療 広汎前立腺切除術	前立腺癌－基礎・臨床研究のアップデート－, 日本臨床	65(10)	331-334	2007
Tateishi U, Onaya H, et al.	Myxoinflammatory Fibroblastic Sarcoma: MR Appearance And Pathologic Correlation	AJR	184	1749-1753	2005

Nara S, Onaya H, et al.	Arterial reconstruction during Pancreato-duodenectomy in patients with celiac axis stenosis- utility of Doppler ultrasonography	Word J Surg	29	885-889	2005
Takahashi Y, Onaya H, et al.	Imaging features of large Intraductal papillary-mucinous carcinoma of the pancreastic tail	Pancreas Apr	32(3)	333-334	2006

Mechanical error analysis of compact forceps manipulator for laparoscopic surgery

[1]Takashi Suzuki, [2]Yoichi Katayama, [3]Etsuko Kobayashi and [3]Ichiro Sakuma
[1]*Advanced Biomedical Engineering and Science, Tokyo Women's Medical University,*
[2]*Graduate School of Frontier Sciences, The University of Tokyo,*
[3]*Graduate School of Engineering, The University of Tokyo*
Japan

1. Introduction

Laparoscopic surgery, sometimes called "keyhole surgery", is one of minimally invasive surgical techniques. All procedures are completed inside abdominal cavity through 3–4 small holes on the abdomen using rigid thin videoscope and long-handled surgical instruments such as clamp, scissors, and scalpel. This patient-friendly technique has a lot of merits compared with conventional laparotomy; less pain, shorter hospital stay, and lower medical costs. It is, however, a difficult procedure. As the linear-shape forceps are bound at the incision hole, symmetrical motion is required around the fulcrum. Surgeons have only four Degrees of Freedom (DOF); two DOFs are for the orientation of forceps, and the other two for axial rotation and longitudinal translation of forceps (Fig. 1), so that laparoscopic surgery needs highly-skilled surgeons with enough experiences.

As one of engineering solutions responding to these clinical issues, surgical manipulators are developed and some of them, such as da Vinci® Surgical System, are clinically applied. These manipulators are aiming to enhance surgeons' ability and dexterity, not for automatic robot surgery. While great contribution to high-quality surgical procedure using three-dimensional view and dexterous robotic hands, one of the drawbacks of surgical manipulators is their size. Conventional operating theatre is too small to install the robotic surgery system. Thus, space-saving, miniaturized manipulator is required.

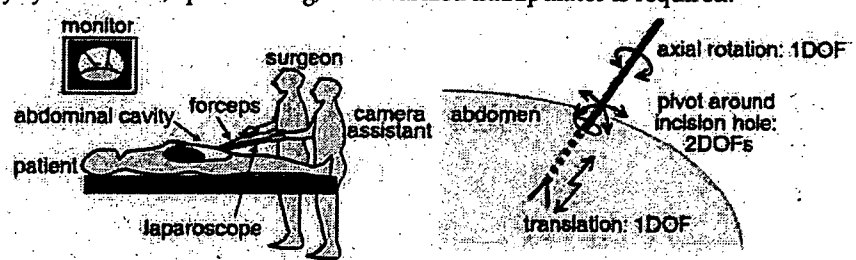

Figure 1. Laparoscopic surgery; surgeon manipulates forceps watching video from laparoscope controlled by camera assistant (left). Limitation of degrees of freedom (rotation, translation, and pivot) is one of causes that make laparoscopic surgery difficult for surgeon (right)

Source: Medical Robotics, Book edited by Vanja Bozovic, ISBN 978-3-902613-18-9, pp.526, I-Tech Education and Publishing, Vienna, Austria

We have developed a compact forceps manipulator using "friction wheel mechanism" (FWM) and "gimbals mechanism" (Suzuki, et al., 2002) and evaluated it (Suzuki, et al., 2005). In this paper, we 1) introduce the mechanism of the manipulator and 2) describe the mathematical analysis of the mechanical error and correction factor based on mechanism of manipulator and the measured error.

2. Method

2.1 Mechanical configuration

In laparoscopic surgery, at least four DOFs are required for forceps motion: axial rotation and longitudinal translation of the forceps, and pivot motion around the incision hole on the abdomen (Fig. 1). We realize only four DOFs because redundancy may disturb the miniaturization and simplification of mechanism; those are important factors for clinical application and commercialization. The compact forceps manipulator we have developed consists of two mechanical subcomponents; Friction Wheel Mechanism (FWM) and Gimbals mechanism. The FWM provides axial rotation and longitudinal translation of forceps using friction drive mechanism. Gimbals mechanism realizes pivot motion of forceps. The prototype is shown in Fig. 2. Dimensions of manipulator are 80×150×320 mm³ and weight is 1.7 kg.

2.2 Friction wheel mechanism

Friction wheel mechanism consists of a couple of friction wheel that has three tilted driving rollers and outer case (Fig. 3).

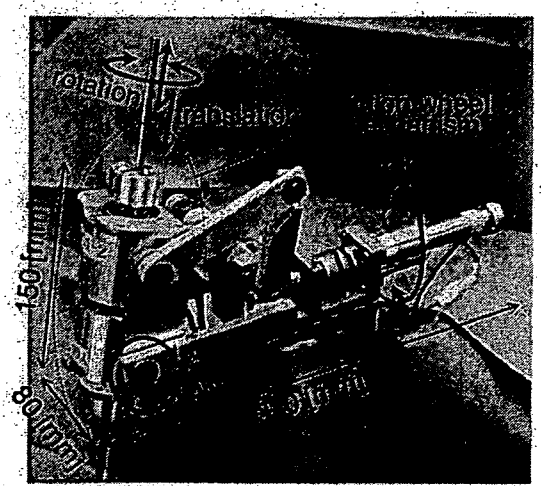

Figure 2. Prototype of compact forceps manipulator; friction wheel mechanism provides rotation and translation of forceps, gimbals mechanism realizes pivot motion (roll, pitch)

Three rollers are radially-located in the case with 120-degree gap, and the forceps shaft is inserted among those rollers. When the outer case is rotated, the rollers travel on the surface of forceps spirally. The shaft is relatively driven by the driving rollers using friction force between rollers and surface of forceps in spiral trajectory. We adopted hollow-shaft

ultrasonic actuators with optical encoder (rated torque 50mNm, custom order, Fukoku, Japan) because of various advantages of ultrasonic motor; compact size and light weight for miniaturization, high holding torque, clean environment for future clinical application, and suitable for hollow-shaft configuration. We use a couple of friction wheels with opposite tilting angle. They provide symmetrical spiral motions like right-handed and left-handed screws, and they are combined to generate rotation and translation (Fig. 4).

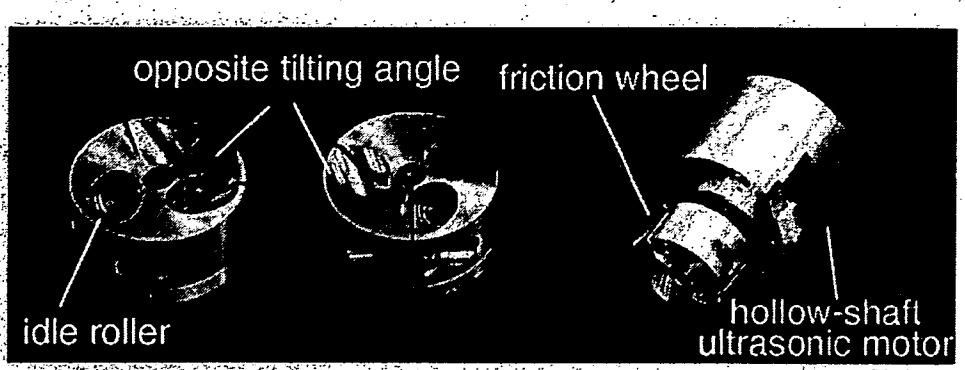

Figure 3. A couple of friction wheel; Each friction wheel has three tilted driving rollers with opposite tilting angle (left). Hollow-shaft ultrasonic motor is adopted for actuation (right)

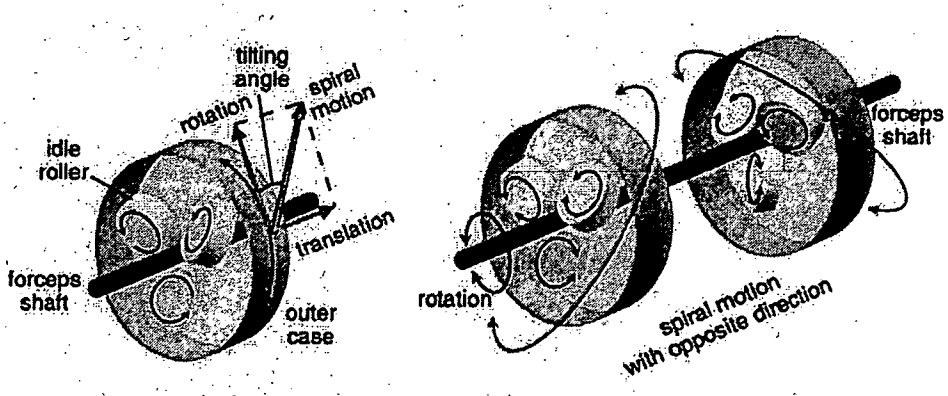

Figure 4. Friction wheel mechanism; friction wheel travels spirally around the forceps shaft (left). Opposite tilting angle generates two different spiral shapes like right-handed and left-handed screws (right)

For the axial rotation of forceps shaft, two friction wheels are rotated in the same direction. In that case, driving rollers and shaft does not have relative speed, so that spiral motions are not generated and forceps shaft rotates at the same speed of friction wheel. For the longitudinal translation, two friction wheels are rotated in the opposite direction. In this case, spiral motions are generated. The rotational components of spiral motion are cancelled mutually and remaining translation drives the forceps (Fig. 5).
The mechanism to generate translation can be shown using mathematical expression (Fig. 6).

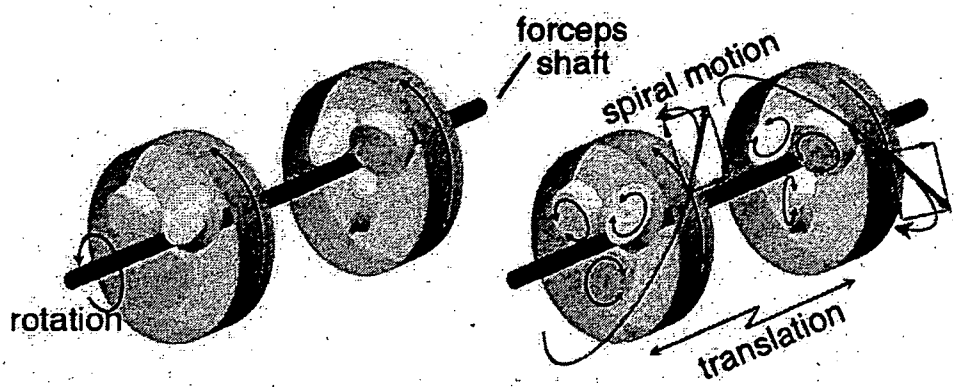

Figure 5. Driving principle of friction wheel mechanism: Rotational motion is generated by rotating both motors in the same direction (left). When each motor is driven in the opposite direction, rotational motions are cancelled mutually and remaining translational motion drives forceps in the longitudinal direction (right)

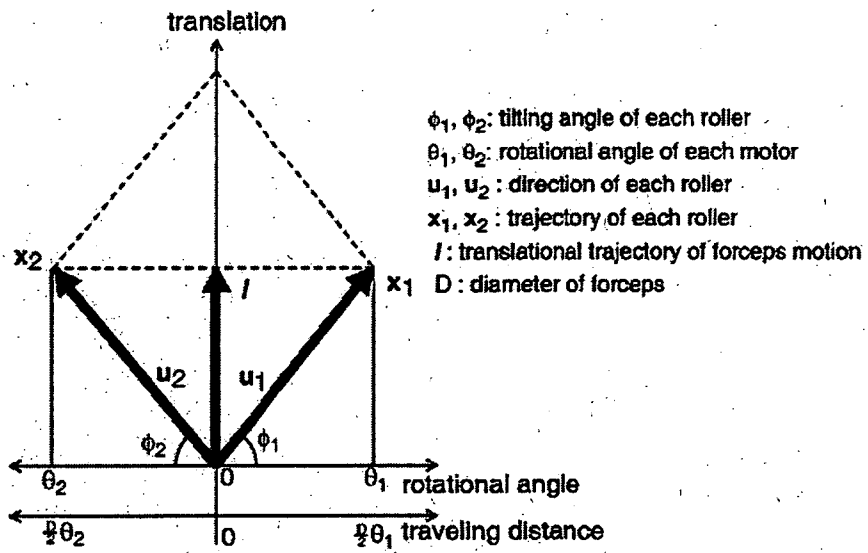

Figure 6. Translational motion can be shown by expanding the surface of forceps to a plane Here, each roller has tilting angle of ϕ_1 and ϕ_2. When outer cases are rotated by θ_1 and θ_2, trajectory of each roller is as follows;

$$\begin{cases} x_1 = \frac{D}{2}\theta_1 u_1 = \frac{1}{2}\begin{bmatrix} D\theta_1 \\ D\theta_1 \tan(\phi_1) \end{bmatrix} \\ x_2 = \frac{D}{2}\theta_2 u_2 = \frac{1}{2}\begin{bmatrix} D\theta_2 \\ D\theta_2 \tan(\phi_2) \end{bmatrix} \end{cases} \quad (1)$$

As the traveling distance is written as the average of two friction wheels, translation can be express using rotational angle of each motor (θ_1 and θ_2) and tilting angle (ϕ_1 and ϕ_2);

$$
\begin{aligned}
l &= \frac{x_1 - x_2}{2} \\
&= \begin{bmatrix} \frac{D}{4}(\theta_1 - \theta_2) \\ \frac{D}{4}(\theta_1 \tan(\phi_1) + \theta_2 \tan(\phi_2)) \end{bmatrix} \\
&= \begin{bmatrix} \frac{D}{4}(\theta_1 - \theta_2) \\ \frac{D}{4}(\theta_1 + \theta_2)\tan(\frac{\pi}{6}) \end{bmatrix} \qquad \left(\phi_1 = \phi_2 = \frac{\pi}{6}\right) \\
&= \begin{bmatrix} 0 \\ \frac{D}{2}\theta \tan(\frac{\pi}{6}) \end{bmatrix} \qquad \left(\theta_1 = \theta_2 = \theta\right)
\end{aligned} \tag{2}
$$

Here, we used 30 deg ($\pi/6$ rad) for tilting angle of rollers and θ for rotational angle of each motor. As shown in eq. (2), the translational distance is controlled by the rotational angle of actuator like a ball screw.

This mechanism is proposed by Vollenweider for surgery simulator (Vollenweider, et al, 1998). Ikuta, et al. also adopted the similar mechanism for axial rotation and longitudinal translation of colonoscope in the virtual endoscope training system (Ikuta, et al., 1998). To the best of authors' knowledge, this is the first prototype that uses this kind of rotation and translation mechanism not for simulator but for real manipulator.

2.3 Gimbals mechanism

Gimbals mechanism has two mutually-perpendicular intersectional rotational axes and realizes pivoting motion of forceps with wide working range around the trocar port. The simple kinematics eases numerical control.

A concern about the location of rotational centre of the mechanism should be discussed. Many studies have proposed the necessity of the remote centre of motion (RCM) mechanism to realize pivot motion with no mechanical part at the trocar port; such as R-guide (Mitsuishi, et al., 2003) and parallel-linkage mechanism (Taylor, et al., 1995, Madhani, et al., 1998, and Kobayashi, et al., 2002). As gimbals mechanism has its rotational centre inside it, not at the incision hole, the rotational centre is located above trocar port and forceps pulls abdominal wall accompanying its pivot motion. As we reported in the past publication (Suzuki, et al., 2002), the result of preliminary in-vivo experiment using pig showed no problem; such as expansion of incision hole and bleeding. We conclude that gimbals mechanism will not damage the abdominal wall because abdominal muscle got relaxed under anaesthesia and incision hole follows the motion of forceps, although the required torque increased to pull the abdominal wall according to the pivot motion of forceps and actuators should be carefully selected. We adopted DC servomotor (ENC-185801, CITIZEN CHIBA PRECISION Co., LTD) to control each rotational axis.

3. Evaluation

3.1 Separation between translation and rotation

One of advantages of FWM is that it realizes rotation and translation with one miniaturized mechanism. For appropriate rotation and translation, we need two conditions; one is the shape of each spiral and the other is rotational speed of each motor. In other words, the lead length of each spiral motion generated by friction wheel should be the same, and rotational speed of each motor should be the same. This is because rotational component of spiral motion must be the same to be cancelled mutually. Our former studies, however, showed that the friction wheel mechanism provided rotational error in translation. We measured the rotational error when 90 mm translation, equivalent to 1800 deg rotation of actuator, was input. The rotating angle of each actuator was controlled using pulse signal from rotary encoders mounted on the motor. The rotating angle of forceps shaft was measured using digital microscope (VH-7000C, Keyence, Japan) with 0.5 deg resolution. The result of error evaluation is shown in Table. 1 (Suzuki, et al., 2005). Measured error was large compared to the required specification we set for this manipulator.

input	error factor	required spec.	average +/- S.D.
translation (90 mm, 1800 deg)	rotation	less than1 deg	14.5 +/- 3.0 deg

Table 1. Rotational error of friction wheel mechanism in translational input

3.2 Error analysis based on mechanical error

For the error correction, we analyze the cause of rotational error in translational motion. As mentioned above, the error motion is caused by different spiral shape generated by each friction roller and/or different rotating angle of each actuator. As we control the actuators using rotary encoders, we can omit the possibility of different rotating angle. Thus, the cause of unstable motion is mismatch of lead length between each friction roller. Lead length error is caused by tilting angle error of the friction rollers. The angle error is determined by the machining error in prototyping process.

We discussed the cause of rotational error in translation and its correction method based on the mechanism of friction wheel. Error analysis is shown here using Fig. 7.

Rotational error is shown as follows;

$$\Delta\theta=\frac{1}{2}(\hat{\theta}_1-\hat{\theta}_2) \tag{3}$$

Because the forceps shaft is rigid, the translational distance generated by each roller is the same, and sum of rotational angle are the same between each roller.

$$\begin{cases} \hat{\theta}_1\tan(\phi+\Delta\phi_1) = \hat{\theta}_2\tan(\phi+\Delta\phi_2) \\ \hat{\theta}_1+\hat{\theta}_2 = \theta_1+\theta_2 \end{cases} \tag{4}$$

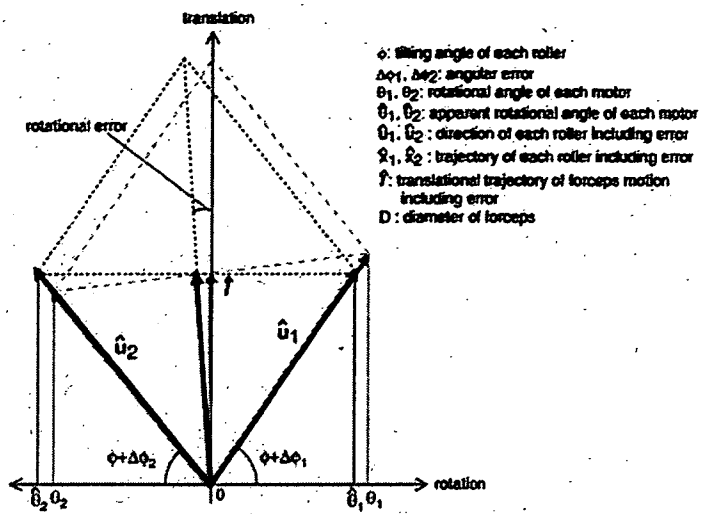

Figure 7. Error analysis of rotational error in translational motion

When these simultaneous equations (4) are solved for $\hat{\theta}_1$ and $\hat{\theta}_2$, they are shown as follows;

$$\begin{cases} \hat{\theta}_1 = \dfrac{\tan(\phi+\Delta\phi_2)}{\tan(\phi+\Delta\phi_1)+\tan(\phi+\Delta\phi_2)}(\theta_1+\theta_2) \\ \hat{\theta}_2 = \dfrac{\tan(\phi+\Delta\phi_1)}{\tan(\phi+\Delta\phi_1)+\tan(\phi+\Delta\phi_2)}(\theta_1+\theta_2) \end{cases} \tag{5}$$

Consequently, $\Delta\theta$ (eq. (3)) is shown using eq.(5).

$$\begin{aligned} \Delta\theta &= \frac{1}{2}(\hat{\theta}_1-\hat{\theta}_2) \\ &= -\frac{1}{2}\frac{\tan(\phi+\Delta\phi_1)-\tan(\phi+\Delta\phi_2)}{\tan(\phi+\Delta\phi_1)+\tan(\phi+\Delta\phi_2)}(\theta_1+\theta_2) \end{aligned} \tag{6}$$

This means that the rotational error is proportional to the sum of input rotating angle (θ_1, θ_2), and that the coefficient is determined using only mechanical error of tilting angle ($\Delta\phi_1$ and $\Delta\phi_2$), thus the error could be compensated using correction factor. On the assumption that rotational error of $\Delta\theta$ is observed when angle of θ_0 is input to generate translation, the correction factor is analyzed. As the condition, we have following equations. Equation (7) means the translational distance is expressed in two ways. The first equation in eq.(8) means input angle for each driving roller is the same in the case of translational input, and other equations are geometrically trivial.

$$\hat{\theta}_1\tan(\phi+\Delta\phi_1)=\frac{1}{2}\left(\theta_1\tan(\phi+\Delta\phi_1)+\theta_2\tan(\phi+\Delta\phi_2)\right) \tag{7}$$

$$\begin{cases} \theta_1 = \theta_2 &= \theta_0 \\ \tan(\phi+\Delta\phi_1) &= \dfrac{\hat{l}}{\hat{\theta}_1} \\ \tan(\phi+\Delta\phi_2) &= \dfrac{\hat{l}}{\hat{\theta}_2} \end{cases} \tag{8}$$

When equations (8) are assigned to eq.(6) and (7), $\hat{\theta}_1/\theta_0$ and $\hat{\theta}_2/\theta_0$ are shown as eq.(9).

$$\begin{cases} \dfrac{\hat{\theta}_1}{\theta_0} = \dfrac{-2k+1+\sqrt{4k^2+1}}{2} \\ \dfrac{\hat{\theta}_2}{\theta_0} = \dfrac{2k+1+\sqrt{4k^2+1}}{2} \\ \qquad (k=\Delta\theta/\theta_0) \end{cases} \Rightarrow \begin{cases} \dfrac{\hat{\theta}_1}{\theta_0} = 1-k \\ \dfrac{\hat{\theta}_2}{\theta_0} = 1+k \\ \qquad (k \ll 1) \end{cases} \tag{9}$$

As they are the error coefficient of driving rollers, the inverse of those coefficients are the correction factor C_1 and C_2 (eq.(10)).

$$\begin{cases} C_1 = \dfrac{\theta_0}{\hat{\theta}_1} = \dfrac{1}{1-k} = 1+k \\ C_2 = \dfrac{\theta_0}{\hat{\theta}_2} = \dfrac{1}{1+k} = 1-k \\ \qquad\qquad\qquad\qquad (k \ll 1) \end{cases} \tag{10}$$

Consequently, the correction factor can be expressed using k that is determined by input angle ($\Delta\theta$) and measured error angle (θ_0).

3.3 Re-evaluation of separation after compensation

We measured rotational error again. In this measurement, we applied the correction factor k by assigning 1800 deg to θ_0 and 14.5 deg to $\Delta\theta$. Result is shown in Table 2 comparing the result of the case without correction factor. The rotational error was reduced more than 90 % by the error correction factor (Suzuki, et al., 2005).

input	error factor	correction factor	average +/- S.D (deg)
translation (90 mm, 1800 deg)	rotation	without	14.5 +/- 3.0
		with	1.0 +/- 1.0

Table 2. Rotational error of friction wheel mechanism in translational input with/without correction factor

4. Discussion

For realization of stable forceps manipulation using friction wheel mechanism, we analyzed the mechanical configuration of manipulator and proposed a correcting factor based on the input rotating angle and measured rotational error, so that the error was reduced by 90%. When the 90 mm translation is input, the error was approximately 1.0 deg. In laparoscopic surgery, innermost target is sometimes located 300 mm from incision hole. In that case, the rotational error will increase up to approximately 3.0 deg. As it does not meet the required specification of 1deg accuracy, we have to find other causes of unstable motion.

One of possible causes is the variation of correction factor. We calculated the correction factor as a constant value from limited number of sets of measured error and input rotating angle. The error correction factor may change depending on the surface condition of forceps shaft, so we need to change correction factor dynamically. Another cause is slip between friction rollers and forceps shaft. In the current prototype, the forceps position is calculated from encoder value and controlled in semi-closed feedback loop. We do not consider position error caused by slight slip or its accompanying accumulated error.

These issues could be solved by closed feedback control loop using direct sensing of forceps position. As implementation methods, we can use three dimensional optical position sensor and/or texture recognition system like optical mouse.

5. Conclusion

In this study, we introduce a compact forceps manipulator with four DOFs for laparoscopic surgery. It consists of two mechanical parts; friction wheel mechanism and gimbals mechanism. Friction wheel mechanism is space-saving and realizes two degrees of freedom of rotation and translation using a couple of friction wheel. Gimbals mechanism realizes wide working range and easy control. One of the drawbacks of FWM, rotational motion error in translational input, was shown and analyzed mathematically based on the mechanical configuration of manipulator. Rotational error was reduced more than 90 % by the error correction factor calculated from the mathematical analysis of mechanical configuration.

In the future works, we will work to modify mechanical configuration based on the results of this study and improve control method from semi-closed feedback control using rotary encoders to closed feedback control using direct position sensing method, such as three-dimensional optical position sensor. As another future work, we will integrate this forceps manipulator with robotized forceps, such as laser coagulator forceps with CCD camera (Suzuki, et al., 2004).

6. Acknowledgement

This work is partly supported by following grants;
-"Research for the Future Program (JSPS-RFTF 99I00904)" funded by Japan Society for the Promotion of Science
-Electro-Mechanic Technology Advancing Foundation
-"Research and Development of the Compact Surgical Robot System for Future Medical Care" funded by New Energy and Industrial Technology Development Organization (NEDO)

-"Research on medical devices for analyzing, supporting and substituting the function of human body" funded by Ministry of Health, Labour and Welfare
-JPSP(#18680041).

7. References

Ikuta, K. et al (1998). Virtual Endoscope System with Force Sensation. In :*Proceedings of the first international conference on medical image computing and computer-assisted intervention - MICCAI98, Lecture Note in Computer Science* 1496, pp.293-304, ISBN:3-540-65136-5, Cambridge, MA, USA, October, 1998, Springer.

Kobayashi, Y. et al (2002). Small Occupancy. Robotic Mechanisms for Endoscopic Surgery. In : *Proceedings of the 5th international conference on medical image computing and computer assisted intervention* (MICCAI2002), *Part 1, Lecture Note in Computer Science* 2488, ISBN:3-540-44225-1, Tokyo, Japan, September, 2002, Springer.

Madhani, A. et al (1998). The Black Falcon: a teleoperated surgical instrument for minimally invasive surgery. In : *Proceedings of IEEE/RSJ international conference on intelligent robots and systems – IROS1998, vol.2,* pp.936-944, Victoria, BC, Canada, 1998, October, IEEE.

Mitsuishi, M. et al (2003). Development of a remote minimally-invasive surgical system with operational environment transmission capability. In :*Proceedings of the 2003 IEEE international conference on robotics and automation - ICRA2003,* pp. 2663-2670, Taipei, Taiwan, September, 2003, IEEE.

Suzuki, T. et al (2002). A new compact robot for manipulation forceps using friction wheel and gimbals mechanism. In : *Proceedings of the 16th international congress and exhibition computer-assisted radiology and surgery - CARS2002,* pp.314-319, ISBN:3-540-43655-3, Paris, France, 2002, June, Springer.

Suzuki, T. et al (2004). Development of a robotic laser surgical tool with an integrated video endoscope. In :*Proceedings of the 7th international conference on medical image computing and computer assisted intervention*–MICCAI2004, *Part II, Lecture Note in Computer Science* 3217, pp.25-32, ISBN:3-540-22977-9, Saint-Malo, France, September, 2004, Springer.

Suzuki, T. et al (2005). Compact forceps manipulator using friction wheel mechanism and gimbals mechanism for laparoscopic surgery. In :*Proceedings of the 8th international conference on medical image computing and computer assisted intervention–MICCAI2005, Part II, Lecture Note in Computer Science 3750,* pp.81-88, ISBN:978-3-540-29326-2, Palm Springs, CA, USA, October, 2005, Springer.

Taylor, RH. et al (1995). A telerobotic assistant for laparoscopic surgery. *IEEE Engineering in Medicine and Biology Magazine,* vol.14, no.9, May/Jun 1995, pp.279-288, ISSN:0739-5175.

Vollenweider, M. et al (1998). Surgery simulator with force feedback. In :*Proceedings of the 4th international conference on motion and vibration control - MOVIC98,* Zurich, Switzerland, 1998.

CHAPTER 7

METHODS IN COMBINED COMPRESSION AND ELONGATION OF LIVER TISSUE AND THEIR APPLICATION IN SURGICAL SIMULATION

ICHIRO SAKUMA
Department of Precision Engineering
School of Engineering, The University of Tokyo
7-3-1 Hongo Bunkyo-ku, Tokyo 113-8656, Japan
sakuma@miki.pe.u-tokyo.ac.jp

CHEEKONG CHUI
Institute of Environmental Studies
Graduate School of Frontier Sciences, University of Tokyo
7-3-1 Hongo Bunkyo-ku, Tokyo 113-8656, Japan
and
Department of Mechanical Engineering
National University of Singapore, E3-05-23 Engineering Drive 3
Singapore 119260, Singapore
mpecck@nus.edu.sg

A fundamental problem in computer aided surgical simulation is soft tissue modeling. It is difficult to represent the complex biomechanical properties and yet computational efficient for fast simulation. This paper reviews the methodologies for determination of the elastic properties of porcine liver tissues. The combined compression and elongation test is used as a unified framework to study the liver biomechanics for computer aided surgical simulation. At a length scale of approximately 10 mm, liver tissue is incompressible, anisotropic and nonlinear viscoelastic. It is stiffer during compression. The tissue sample will buckle under a mean stress of 2.313×10^5 Pa under compression. The Poisson's ratio was 0.466 ± 0.147 during compression and 0.431 ± 0.155 during elongation. Constitutive laws including strain energy based combined energy equation and equivalent stress and stain based multi-linear model were used in modeling the nonlinear stress-strain behavior of liver tissues under compression and elongation. Application of the experimental data and theoretical models is demonstrated via finite element simulation of liver organ deformation.

1. Introduction

Computer aided surgery (or computer integrated and robot assisted surgery) is performed to satisfy unmet complex needs in surgeries such as image guided surgeries. Image guided surgeries or minimally invasive surgeries are becoming increasingly popular. In an image guided surgery, the surgical procedure is facilitated by a real time correlation of the operative field to a monitor, which shows the

precise location of a selected surgical instrument to the surrounding structures. This is different from the conventional open surgery in which the surgeons can see the tissue being operated on directly. The image guided surgery is both beneficial to patients and cost-effective, and is fast becoming the standard of care for various surgeries.[1]

A computer aided surgery process is complex. In a typical process shown in Fig. 1, its components include preoperative imaging, modeling and segmentation, simulation, then registering sources of data and applying these to the intervention on the patient. The interventions are monitored, corrected, or extended, according to the results of intraoperative imaging. Virtual reality-based simulation of image guided surgery has been reported by various investigators. Virtual reality techniques[2] and the emergence of automatic surgical tools and robots[3] have been driving an exciting area of research–computer simulation of surgical procedures or computer aided surgical simulation.

Virtual reality and simulator-based technology systems have significant practical value in training and in evaluating user responses in situation-specific problem solving for both the military and industrial sectors.[4,5] It is only natural that this technology be utilized for medical applications. For example, the various surgical simulation systems for interventional radiology, cardiology and neuroradiology reported in Anderson *et al.*[6] and references cited therein focus on training of user skills, improving hand-eye coordination, training of specific patient management decision-making skills, training of very specific specialized skills, and evaluating treatment approaches for patient specific pretreatment planning. There are on-going research efforts to develop patient specific catheterization devices using simulation-based design technology.[7,8] Another application of computer programs enabling accurate modeling of soft tissue deformation is in surgical robot control systems for neurosurgery[9] as well as treatment of liver cancers.[10] Nevertheless, clinical applications of this surgical simulation technology are currently limited.

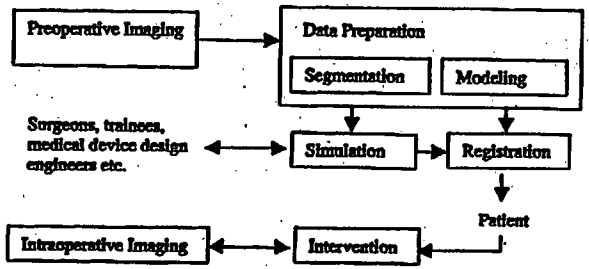

Fig. 1. Typical computer aided surgery process: The focus of this study is on surgical simulation, in particular the biomechanical modeling of liver tissue. Outcome of simulation may be used for training as well as medical device design and evaluation.

As of today, virtual reality is not likely to be found in the operating room.[11] The underlying computer-based anatomical models are not quite realistic enough. There should be a faithful representation of geometry, boundary and loading conditions as well as mechanical properties of the organ. The fundamental problem in anatomical modeling is the lack of "physics" in particular soft tissue modeling of liver, kidney and brain. It is desirable to have the behavior of the object depend on the constitutive properties of the object being simulated. The mechanical properties of liver, kidney and brain tissues are also different. Brain tissue is apparently softer and is more viscous compared to that of liver tissue. Several studies have underlined the importance of duly considering elastic tissue deformation.[12]

Precise information about the elastic properties and corresponding constitutive laws of biological soft tissues determines the performance of surgical simulators. These tissues are highly nonlinear and complex. Quantitative data about the biomechanical properties of soft tissues are few. It is a challenge to derive a representative constitutive law that is clinically relevant as well as computationally efficient for computer aided surgical systems. Basic research and measurement experiments are required to understand and model the biomechanics of soft tissue. The field of biomechanics which is defined as the research and analysis of the mechanics of living organisms places great emphasis on the physiological correctness of the mathematical model. On the other hand, computational efficiency is essential for practical clinical application. The approach employed here involves refining the conventional approaches based on continuum mechanics to measure and model the biomechanics of liver tissue for computer aided surgical simulation.

This paper is organized as follows. In Sec. 2, we discuss the various methods in measuring the mechanical properties of liver tissues with particular focus on the combined compression and elongation test. The combined compression and elongation test enabled zero stress state of the tissue sample to be precisely determined for the tensile test. In Sec. 3, we characterize the mechanical properties of liver tissue. When deformed, kidney and brain will behave differently from liver. It is necessary to have an in-depth investigation on the biomechanical properties of liver on its own. In Sec. 4, the strength and elastic modulus of liver tissues are investigated. Mathematical modeling of liver tissue mechanics is discussed in Sec. 5. It is more beneficial to model the stress–strain behavior from combined compression and elongation test than that of simply compression or simply elongation. Organ deformation involves both compressible and tensile displacement. Depending on the specific applications, the constitutive model used is a trade off between computational accuracy and interactivity. Section 6 describes biomechanical modeling of liver organ and surgical simulation of organ deformation. In surgical simulation, the biomechanical model has to be computationally efficient so that the computer simulation could provide a timely solution. Concludes Sec. 7 with a brief discussion on the future work.

2. Measurement of Liver Tissue Elasticity

The developments in computer aided surgery where precise information about the elastic properties of living tissues are desired fuels the recent interest and progress in measuring the mechanical properties of biological tissues. The emphasis of these measurement methods is on low speed loading condition.

Surgical instruments had been equipped with force-sensing capabilities allowing elasticity measurement during surgeries.[13,14] Pathak *et al.*[15] applied indentation methods for *in vivo* experiments on the skin. However, these techniques lacked well-defined boundary conditions during experiment and often failed to address the complex material properties of tissue with nonlinear constitutive equations. MR elastography[16] was a possible method for non-invasive imaging of elastic properties in non-homogeneous organs. This method spatially maps and quantifies small displacements caused by propagating harmonic mechanical waves. Nevertheless, the resulting very small displacements and frequency range could not predict the tissue behavior in the range of strains and strain rates observed during surgical interventions. Kauer *et al.*[17] presented a tissue aspiration method for *in vivo* determination of the material parameters of biological soft tissue. An explicit axisymmetric finite element simulation of the aspiration experiment is used together with a Levenberge-Marquardt algorithm to estimate the material model parameters in an inverse parameter determination process. This tissue aspiration method with inverse finite element characterization has well defined mechanical boundary conditions and could induce relatively large tissue deformation. However, the condition of axisymmetry assumed in this method could not be met in the measurement experiments since soft tissues are in general anisotropic. Generally, it will be too expensive even if it is possible to generate enough data using *in vivo* measurement experiments to obtain adequate statistical interpretation of the mechanical properties of soft tissue. This is primarily due to the extreme technical and ethical demands on such experiments, and vast diversity in mechanical properties of biological tissues.

Indentation tests were used in Davies *et al.*[18] to determine the mechanical properties of spleen tissue. Tie and Desai[19] reported their indentation experiments to characterize the biomechanical properties of porcine liver tissue. Indentation experiment on whole liver organ with inverse finite element parameters estimation was reported in Onodera *et al.*[20] Inverse finite element parameters estimation has increasingly been used in measurement experiments[21] to help determine the mechanical properties of biological tissues. The tissue indentation equipment is generally customary designed and developed by the investigators. In Onodera *et al.*[20] an exponential strain energy function from Fung[22] was implemented into MARC 7 (MSC Software Corporation, USA), a commercially available finite element package popular for nonlinear analysis to perform inverse finite element parameters estimation. However, tissue indentation could be a complex mathematical problem involving both compressive and tensile properties of tissue. If at all possible, it is difficult to separate the compressive and tensile properties of the tissue samples.

Uniaxial load testing has long been used to measure the mechanical properties of both soft and hard tissues.[23] Miller and Chinzei[24] described a uniaxial compression test to measure the mechanical properties of brain tissue. Uniaxial compression and elongation experiments with porcine liver were reported in Chui *et al.*[25] and Sakuma *et al.*[26] Uniaxial load testing is simple but, nevertheless, provides us with basic and useful information on the mechanical properties of liver tissue. There are extensive reports on uniaxial testing with arterial elasticity, e.g. see Ref. 27 and references cited therein. Extensive uniaxial testing with liver tissue is relatively few. The zero stress state of the tissue sample must be identified for testing. However, this identification may not be easy since the neighborhood of the zero stress state of a soft tissue is soft and difficult to handle. The combined compression and elongation test[25,26] enabled the zero stress state to be precisely determined for the tensile test after the compression cycle. The combined compression and elongation cycle was clearly a simpler method compared to other more elaborated approaches for example the use of laser for initial state estimation.[9,24]

2.1. *Preparation of tissue sample*

Careful tissue sample preparation is necessary because cutting the samples possibly affects the results obtained. For example, particular attention should be paid to the orientation of tissue samples because biological tissues are mostly anisotropic, and their mechanical properties depend on direction. In order to determine a mechanical property as close as possible to that of *in vivo*, it is important to test the tissue fresh and maintain its freshness during experiments.

Fresh porcine livers were purchased from a local slaughterhouse for our measurement experiments. Rat liver organs were used in experiments in the "Virtual Rat" project.[28] However, it is generally believed that the mechanical properties of pig liver are close to those of human liver. The weight of a whole porcine liver was 1.5 ± 0.2 kg. The liver was approximately 210 mm by 330 mm with a thickness of 35 mm. Test samples were cylindrical in shape with a fixed diameter of 7 mm and height ranging from 4.5 mm to 11 mm. Figure 2 illustrates the preparation of cylindrical test sample. To establish maximum bonding between the tissue and the attachment unit, we tested the adhesion between liver tissue and various surfaces including wood, steel, cloth and rubber. Adhesion to the rubber plate was maintained with the highest tension used in our experiments. This was twice that obtained using wood, which had the lowest value. At a temperature of 20 ± 3°C, the surgical bond was able to sustain a stress of up to 380 kg/cm.^{2}

Before testing, liver tissue samples were visually inspected for visible vessels and large porous. Samples with vessel or obvious porous were discarded. Since the samples were rather small at 7 mm diameter and generally less than 10 mm in height, and the fact that they were extracted near the liver surface, we were quite certain that the presence of vessel in sample was not significant.

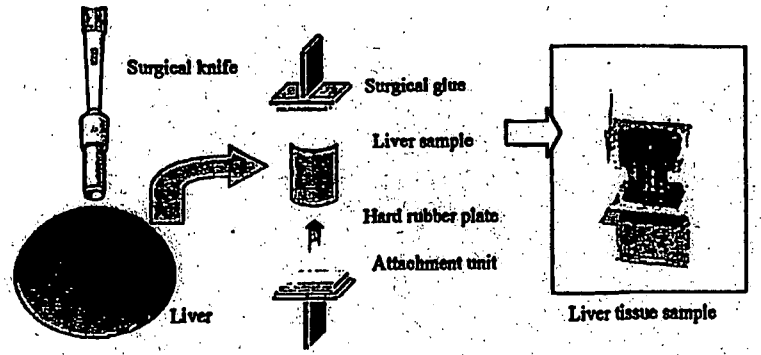

Fig. 2. Overview of cylindrical liver tissue sample preparation:[25] a circular surgical knife is used to extract the tissue sample, and then cut to the desired length using normal surgical knife. Surgical bond (Adhesive A, Sankyo Co. Ltd., Tokyo, Japan) was used to glue the sample to the attachments.

2.2. *Experimental setup*

The test unit was made and placed under a testing machine for experiments. Force and displacement were measured during the loading test by the precision instrument, Eztest, from Shimadzu Co Ltd. of Japan. This instrument had a resolution of ±1%, and could support loading rates ranged from 0.5 to 1000 mm/min. A load cell that was capable of measuring a force up to 20 N was used. A video camera was placed in front of the test sample to record the deformation. The environmental temperature was maintained at about 22°C. Humidity was kept between 60% and 70% to prevent drying of the test pieces.

2.3. *Uniaxial loading tests*

The tests could be classified into following categories: elongation/compression tests, creep tests and relaxation tests. In uniaxial tests, an increasing force is steadily applied to a tissue sample in one direction, and the resulting sample deformation is measured, which gives relations between stress and strain (or stretch ratio). For theoretical treatment, stress and strain in the Lagrangian sense was reference. The tensile or compressive stress T is the load F divided by the cross sectional area A of the sample at zero stress state. The "stretch ratio" or "compression ratio" λ is the ratio of the length or height L of the sample stretched or compressed under the load divided by the initial length L_0 at the zero stress state. Strain ε is the ratio of the displacement $(L - L_0)$ divided by L_0, or $\varepsilon = \lambda + 1$.

Creep and relaxation tests are used for the evaluation of the viscoelasticity or inelastic properties of materials. In the creep tests, tissue sample elongation or compression is measured while a constant static or cyclic force is applied to the sample. In the relaxation test, stress reduction is observed while a tissue sample

is elongated or compressed to a constant length and maintained at that length. Uniaxial tensile or compression testing is the most fundamental method for the determination of the elastic properties of materials, which are evaluated primarily on the basis of stress–strain relations.

In addition to performing the conventional uniaxial elongation and compression tests on liver tissue, force–displacement could be measured during a cycle of compression and elongation. In the combined compression and elongation test, the tissue sample is first compressed and then elongated at the same rate to its stress free position and beyond as illustrated in Fig. 3.

Based on the experimental results, by compressing a cylindrical liver sample of diameter 7 mm by a force of less than 1 N, the tensile test could be started at the zero stress and strain state. Figure 4 compares the measured force–strain data from the elongation only experiments and that of the elongation in the combined

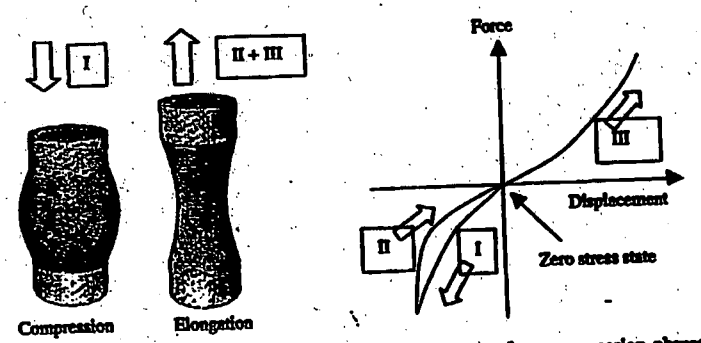

Fig. 3. Illustration of combined compression and elongation test: I — compression phrase; II — return to stress free state; III — elongation phrase.

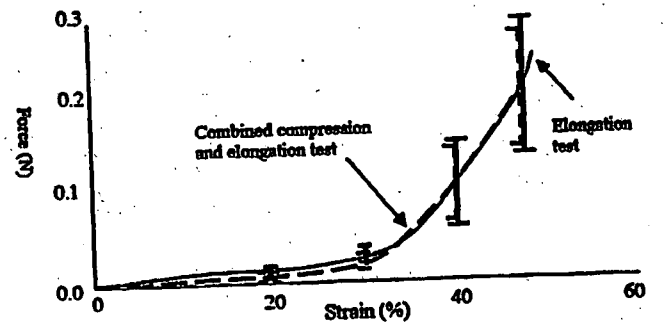

Fig. 4. Comparison of experimental force–strain data from elongation only test and combined compression and elongation test: number of samples = 8, diameter = 7 mm; loading rate = 10 mm/min. Error bar indicates the standard deviation from the average experimental data.

compression and elongation test. The liver tissue samples were compressed up to 0.4 N in the combined compression and elongation test. The measured data between the two experiments are compatible.

3. Characteristics of Liver Tissue

Liver is the second largest organ of the body after the skin. The surface of the liver is covered by a membrane called the visceral peritoneum, also commonly referred to as liver capsule. The liver capsule extends into the substance of liver as highly branched septae. The human liver is comprised of 4 lobes, with the largest two, the right and left lobe, separated by the falciform ligament. The liver lobes are made up of many functional units called lobules. Each hepatic lobule, which is about 1–2 mm in diameter, is a roughly hexagonal arrangement of plates of hepatocytes radiating outward from a central vein in the center. Hepatic lobules are the structural unit of the liver. They are delineated by the connective tissue septae. Detailed description of liver anatomy can be found in Tortora.[29]

3.1. *Stress–strain relationship*

All the liver specimens in our *in vitro* experiment yielded nonlinear stress–strain behavior, having higher distensibility in the low stress range and losing it at progressively higher stresses. Figures 5(a) and 5(b) illustrated typical stress–strain curves of a porcine liver tissue tested in compression and elongation experiments respectively. Each curve could be divided into three parts. In the first part, from O to A (toe region), the load increases exponentially with increasing compression. This is the physiological range in which the tissue normally functions. In the second part, from A to B (linear region), the stress–strain relationship is fairly linear. In the third part, from B to C, the relationship is nonlinear and ends with rupture. B is the yield point. At point C the maximum load is reached, corresponding to the ultimate stress and strain. D is the break point. The slope defined by points A and B is the elastic stiffness from which Young's modulus of liver tissue during compression and elongation are derived respectively if linear elastic model is assumed in computation. Young's modulus or elastic modulus is a measure of the stiffness of a given material. Figure 5(c) shows the average stress–strain curve from combined compression and elongation test of liver tissue samples. The average stress–strain curve is typically used for biomechanical modeling in surgical simulation.

The combined compression and elongation experiments were also performed on kidney and brain tissues. The stress–strain behaviors of liver, kidney and brain tissues are different. Figure 6 compares the average stress–strain data. The brain tissue is significantly softer compared to liver and kidney tissues. Kidney tissue is stiffer than liver tissue.

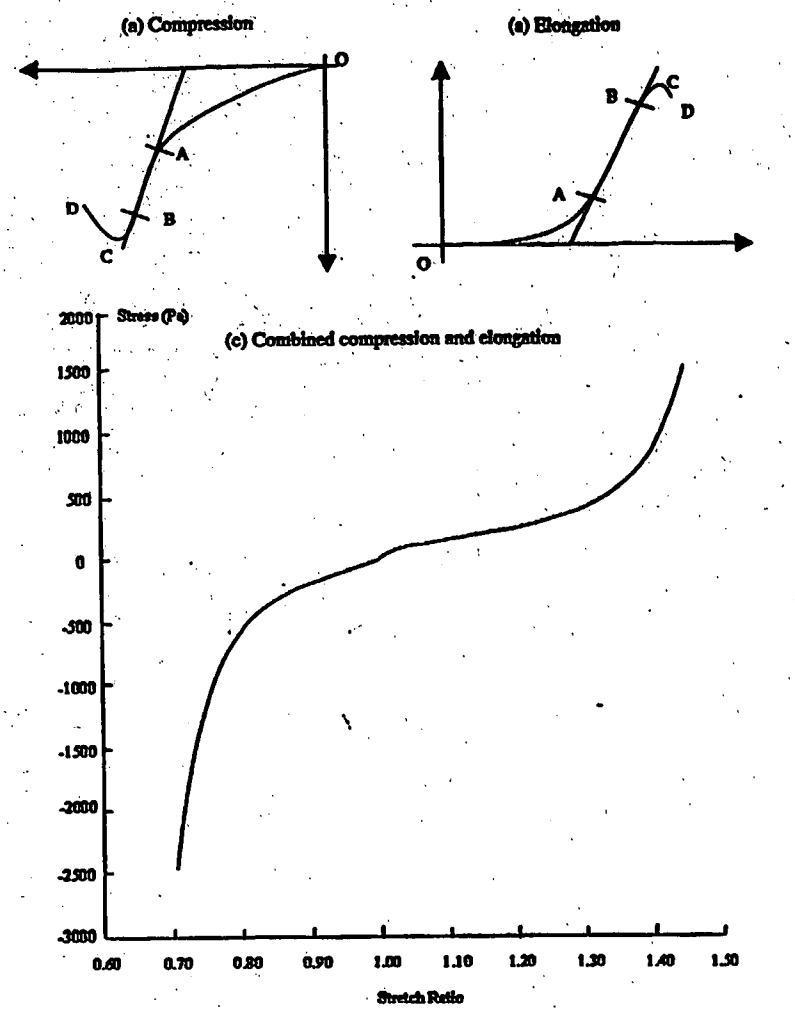

Fig. 5. Typical load–displacement curves of porcine liver tissue until fail during (a) compression and (b) elongation respectively. (c) Average stress–strain curve of combined compression and elongation experiment. Number of samples: 65 from 18 livers. Note that constant loading rate at 10 mm/min is used in all experiments.

3.2. *Nonhomogeneity*

Figure 7 compares the mass density of tissue samples extracted from various parts of a liver organ. Eight groups of samples were extracted from the surface at different locations (A1, A2, B1, B2, C1, C2, D1, D2) in the liver. Mass density is determined